Geochemistry Geophysics Geosystems G3

Article
Volume 14, Number 12
6 December 2013
doi: 10.1002/2013GC004976
ISSN: 1525-2027

Published by AGU and the Geochemical Society

The failed eruption of Mt. Etna in December 2005: Evidence from volcanic tremor analyses

S. Falsaperla, G. Barberi, and O. Cocina

Istituto Nazionale di Geofisica e Vulcanologia, Osservatorio Etneo, Sezione di Catania, Piazza Roma 2, IT-95125, Catania, Italy (susanna.falsaperla@ct.ingv.it)

[1] Strong changes in seismic radiation, comparable to those preceding and/or accompanying eruptive activity in recent years, were recorded at Mt. Etna volcano, Italy, from November 2005 to January 2006. The amplitude of volcanic tremor peaked in mid-December 2005 after a continuous, slow increase from August 2005 onward, during which neither effusive nor paroxysmal activity was observed by volcanologists and alpine guides. During this time span, the centroid locations of volcanic tremor moved toward the surface, more and more clustered below the summit craters. The application of pattern classification analysis based on Self-Organizing Maps and fuzzy clustering to volcanic tremor data highlighted variations in the frequency domain as well. These changes were temporally associated with ground deformation variations, as indicative of a mild inflation of the summit of the volcano, and with a conspicuous increase in the SO_2 plume-flux emission. Overall, we interpret this evidence as the result of recharging of the volcanic feeder at depth (>3 km below sea level) during which magma did not reach the shallow plumbing system.

Components: 9,254 words, 10 figures.

Keywords: time series analysis; volcano seismology; volcano monitoring; neural network and fuzzy logic; seismic tomography.

Index Terms: 7280 Volcano seismology: Seismology; 4302 Geological: Natural Hazards; 8419 Volcano monitoring: Volcanology; 3270 Time series analysis: Mathematical Geophysics; 1872 Time series analysis: Hydrology; 1942 Machine learning: Informatics; 1988 Temporal analysis and representation: Informatics; 4277 Time series experiments: Oceanography: General; 4475 Scaling: spatial and temporal: Nonlinear Geophysics; 0555 Neural networks, fuzzy logic, machine learning: Computational Geophysics.

Received 1 August 2013; **Revised** 18 October 2013; **Accepted** 23 October 2013; **Published** 6 December 2013.

S. Falsaperla, G. Barberi, and O. Cocina (2013), The failed eruption of Mt. Etna in December 2005: Evidence from volcanic tremor analyses, *Geochem. Geophys. Geosyst.*, *14*, 4989–5005, doi:10.1002/2013GC004976.

1. Introduction

[2] Case studies of "failed eruptions," namely episodes of volcanic unrest in which magmatic systems fail to erupt, have recently enjoyed much more interest within the scientific community as an opportunity to learn how volcanoes behave [e.g., *Poland*, 2010; *Moran et al*., 2011]. Seismic monitoring is one of the fundamental pieces of information and a key factor to be considered when a volcano becomes restless and this may highlight dynamics and changes in its internal structure. Besides fracturing events associated with Volcano-Tectonic (VT) earthquakes and signals such as volcanic tremor, which are related to the movement of magmatic fluids [e.g., *McNutt*, 2000], can indeed indicate that magma is forcing its way upward, without necessarily reaching the surface.

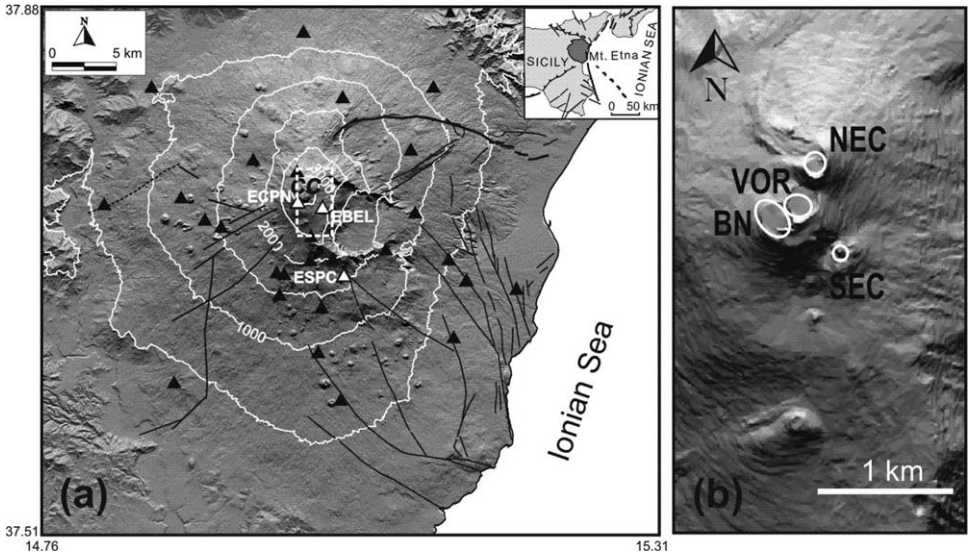

Figure 1. (a) Digital Elevation Model and main faults (in black) in the volcanic body of Mt. Etna (redrawn after *Neri et al*. [2009]). Triangles mark the location of the seismic stations of INGV-OE (EBEL, ECPN, and ESPC are highlighted in white). CC stands for Central Craters. (b) Zoom of the area delimited by the dashed white rectangle in Figure 1a. The white ellipses mark the location of the summit craters: NEC (Northeast Crater), VOR (Voragine), BN (Bocca Nuova), SEC (Southeast Crater).

[3] Mt. Etna is a basaltic stratovolcano which is ideal for studying failed eruptions, as the frequent volcanic activity and continuous seismic monitoring allow us to investigate cases in which changes in activity from seismic baseline do not lead to eruptions. Etna is located in southern Italy along the front of the collision belt between the African and the European plates, at the footwall of a major normal fault system, the Malta Escarpment [e.g., *Hirn et al*., 1997; *Gvirtzman and Nur*, 1999; *Doglioni et al*., 2001]. The volcanic edifice is about 3330 m high; it is crossed by two regional fault systems NNW-SSE and NE-SW oriented, and is characterized by slow and continuous gravitational spreading of its eastern flanks toward South [e.g., *Acocella et al*., 2003; *Walter et al*., 2005; *Solaro et al*., 2010]. Recent lava effusions occurred in 2001, 2002–2003, 2004–2005, 2006, 2008–2009, and their duration varied from about 3 weeks in 2001 to 15 months in 2008–2009 [*Behncke and Neri*, 2003a; *Andronico et al*., 2005; *Burton et al*., 2005; *Aloisi et al*., 2009]. Lavas were erupted by vents located at or nearby the summit craters (the Southeast Crater was the most active in the aforementioned years, Figure 1b) and/or on the flanks of the volcano. Intereruptive periods covered several months, and were punctuated by episodes of lava fountains and strong Strombolian explosions [e.g., *Behncke and Neri*, 2003b; *Di Grazia et al*., 2009]. Here we discuss seismic data collected a few months after the end of the September 2004 to March 2005 effusive activity. We found a conspicuous enhancement of volcanic tremor amplitude which lasted about 3 months. The anomalous increase faded in January 2006, about 6 months before the onset of the July–December 2006 eruptive activity. We analyze the source location of the volcanic tremor centroid and apply pattern classification based on Self-Organizing Maps (SOMs) [*Kohonen*, 2001] and fuzzy clustering [*Zadeh*, 1965] to the frequency content of the background seismic radiation. Finally, we discuss our findings about this "failed" eruption in the light of a recent study in seismic tomography by *Patanè et al*. [2006], imaging the internal structure of the volcano from 7 km below sea level (b.s.l.) up to surface.

2. Data Acquisition

[4] Istituto Nazionale di Geofisica e Vulcanologia, Osservatorio Etneo (INGV-OE) runs 24/7 seismic monitoring of Mt. Etna with a network of broadband and short period sensors in continuous acquisition (Figure 1a). Additionally, seismic arrays are temporary deployed to augment the permanent network. In this study, we particularly refer to two permanent broadband stations (ECPN and ESPC, Figure 1a) equipped with three component Trillium

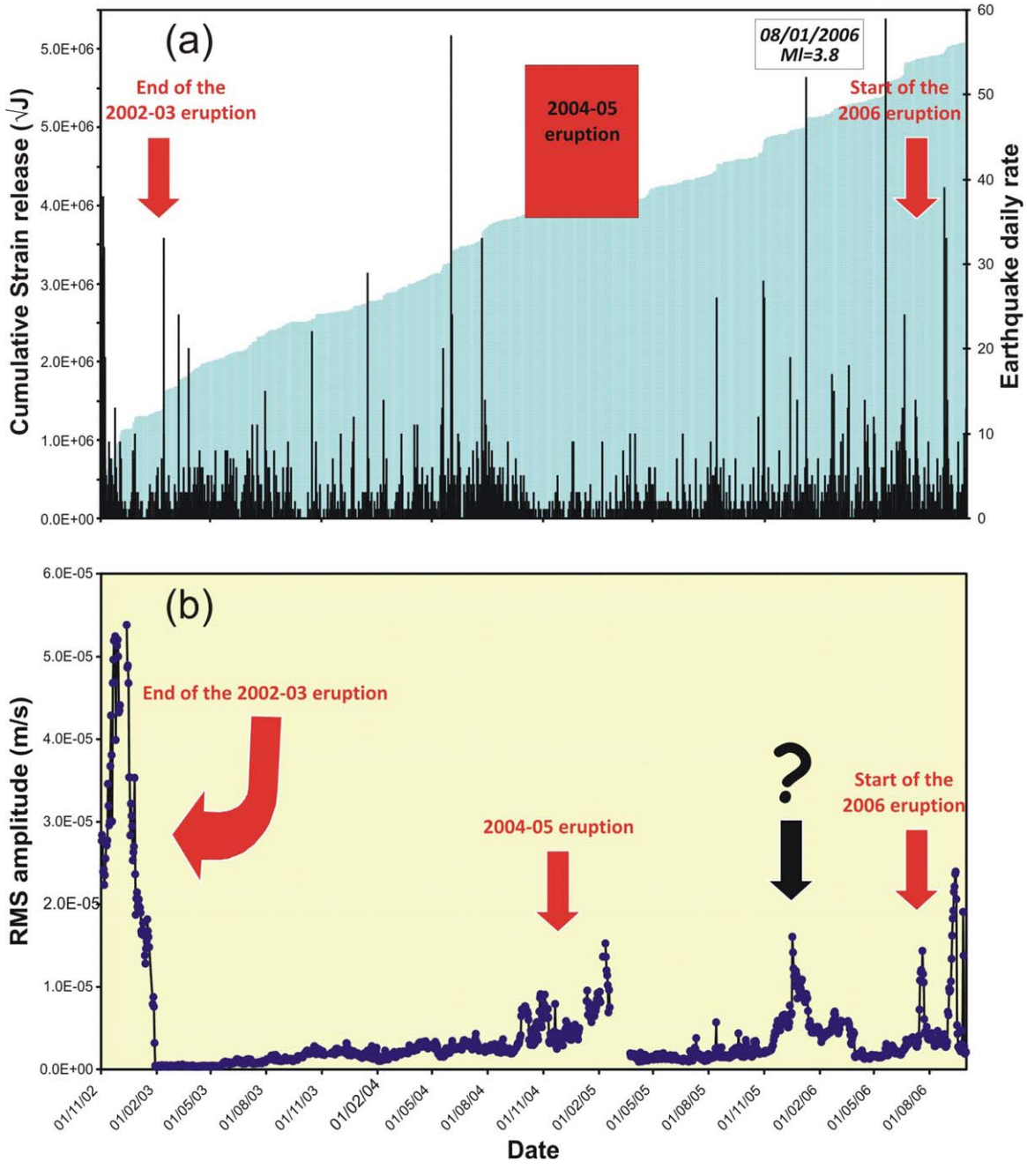

Figure 2. (a) Earthquake daily rate and cumulative strain release, (b) daily amplitude of volcanic tremor at ECPN. The time span ranges from 1 November 2002 to 30 September 2006. Eruptive periods are marked in red. The black arrow in Figure 2b indicates the strong increase in amplitude of seismic radiation in mid-December 2005.

(40 s cutoff period) Nanometrics seismometers. A third station (EBEL) with the same kind of sensors had technical failures from 27 November 2005 to 25 January 2006. We include it in our analysis for its proximity in altitude and location to ECPN (Figure 1a). Seismic signals were sampled at a frequency of 100 Hz and transmitted to Catania, where they were stored in a PC-based acquisition system. The three aforementioned stations were within 3 km (EBEL and ECPN) and 6 km (ESPC) from the summit craters. Their seismic records were corrected for the instrumental response.

3. Seismic Activity

[5] The daily rate of earthquakes between 1 November 2002 and 30 September 2006 is shown

in Figure 2a. There was neither notable change in the number of earthquakes nor in their associated seismic strain release in the second half of 2005 with respect to previous years. The number of earthquakes/day slightly increased in the early 2006, and by 8 January a seismic swarm (maximum magnitude Ml 3.8, Figure 2a) struck the SW flank of the volcano, at a distance of ~8 km from the summit craters and in a depth range between 10 and 14 km (supporting information Figure S1[1]). In total, 408 earthquakes with magnitude $1 \leq Ml \leq 3.8$ were located in the volcanic area from 1 July 2005 to 31 January 2006 (supporting information Figure S1), using phase picks from both permanent and mobile seismic stations. For their location, SIMULPS-14 [*Thurber*, 1993] and the 3-D velocity model by *Patanè et al*. [2006] were applied. Foci ranged from a few hundred meters below the surface to ~26 km b.s.l. Unlike the relatively low rate of VT earthquakes, a high number of long-period (~0.2–2.5 s) and very long-period (~10–20 s) events was recorded between summer and fall 2005. An in-depth description of the characteristics of these events and their temporal evolution are provided by *Cannata et al*. [2009]. A moderate increase in the amplitude of volcanic tremor also started in mid-November 2005 along with variations recorded at permanent GPS stations as indicative of a mild inflation at the summit of the volcano (M. Mattia, personal communication, 2011). The average daily amplitude of volcanic tremor at the vertical component of ECPN from 1 November 2002 to 30 September 2006 is shown in Figure 2b. We observe that tremor amplitude underwent a big change during the three eruptions in 2002–2003, 2004–2005, and from July 2006 on. Between November 2005 and January 2006, the amplitude of seismic radiation was generally greater at ECPN, with the exception of a few episodes from 16 to 25 November (Figure 3a). These episodes were more energetic at EBEL and ESPC than ECPN. Based on the root mean square (RMS) amplitude calculated over consecutive 5 min intervals, Figure 3a shows the bottom 10% (10th percentile) of the amplitude of the signal in order to remove any undesired transient event; amplitudes were normalized to the maximum value reached in each station. During the night of 16 December, the energy of seismic radiation abruptly increased (see also seismogram in Figure 4a). The climax

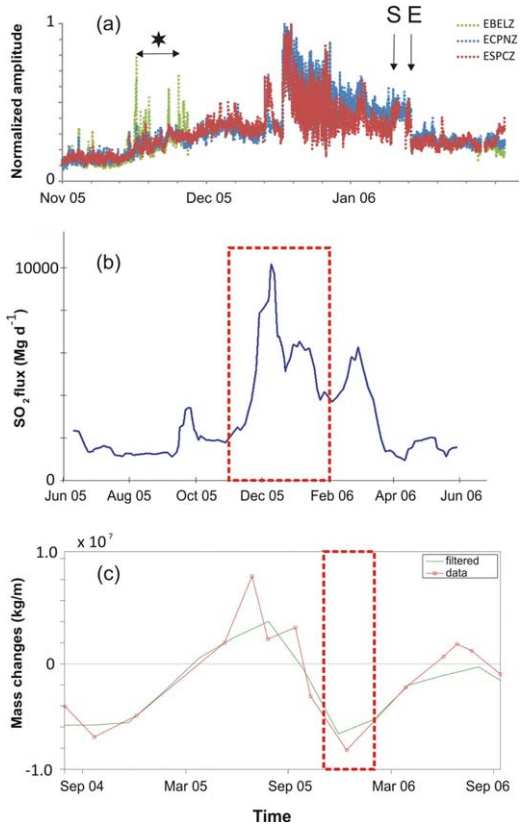

Figure 3. (a) Amplitude of volcanic tremor at the vertical component of ECPN, EBEL, and ESPC between November 2005 and January 2006. For each station, amplitudes are normalized to the maximum value. (b) SO_2 flux from 1 June 2005 to 31 May 2006. (c) Mass changes (mass per unit length) in the southern flank of Etna from September 2004 to September 2006 (modified from *Greco et al*. [2010]). The dashed, red rectangle in Figures 3b and 3c covers the three-month time span reported in Figure 3a. The black star in Figure 3a refers to the time span from 16 to 25 November when the amplitude of seismic radiation temporary peaked at EBEL. Black arrows mark in Figure 3a the occurrence of the seismic swarm (S) and strong explosion (E) on 8 and 12 January 2006, respectively.

achieved amplitudes of ~1.9×10^4 nm/s at ECPN, typical of eruptive stages before and after December 2005 (Figure 2b); however, no eruption occurred. The RMS amplitude remained high until 18 December, and then gradually decreased. By 18 December, periodic bursts of tremor were recorded in the form of "banded tremor," unveiling a cyclic behavior common in geothermal systems like geysers [*Kieffer*, 1984] and reported in several basaltic volcanoes, such as Kilauea (Hawaii), Pavlof (Alaska), and Oshima (Japan) [*McNutt*, 1992]. The phenomenon continued until 27 December, with "bands" of enhanced energy

[1]Additional supporting information may be found in the online version of this article.

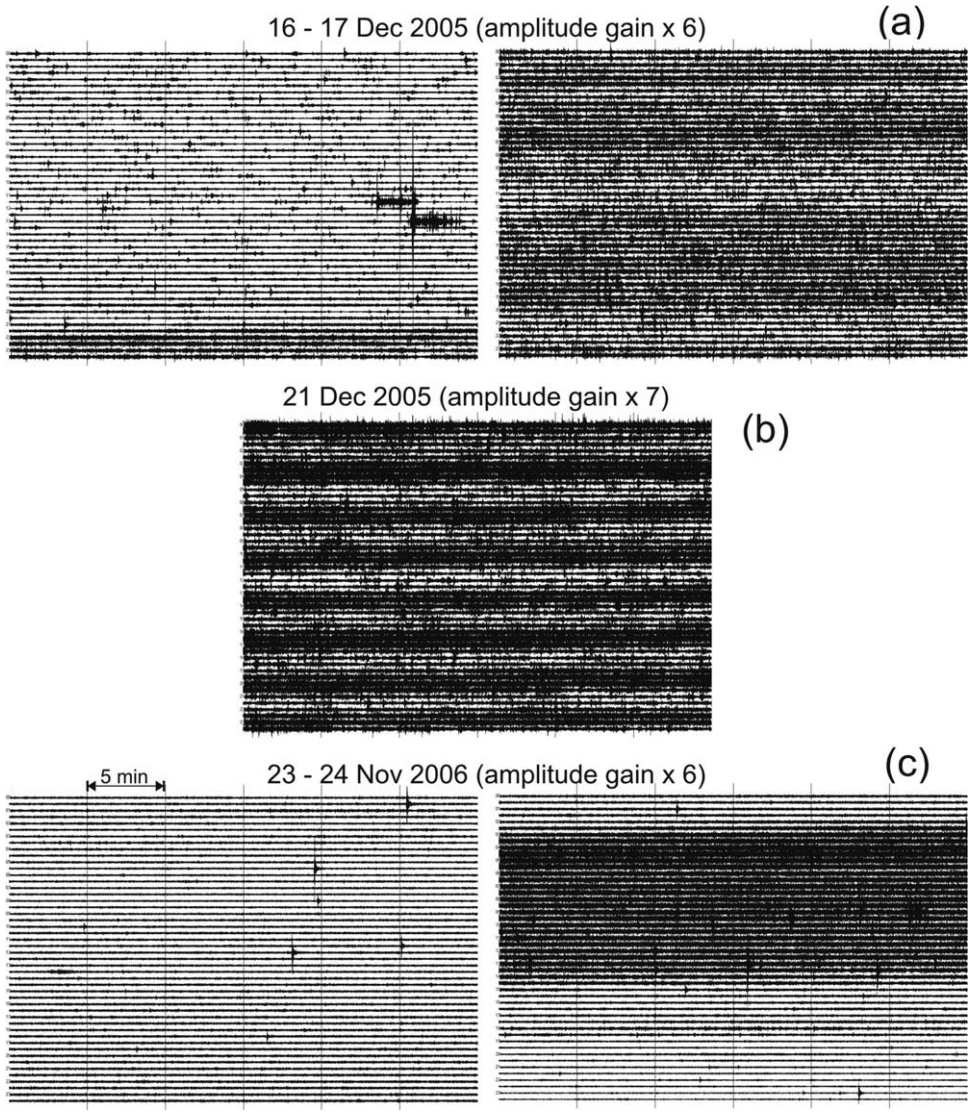

Figure 4. Seismograms of (a) 16–17 December 2005, (b) 21 December 2005, and (c) 23–24 November 2006 at ECPN. (b) Example of "banded tremor." Each seismogram covers 24 h. Eruptive activity occurred only in Figure 4c.

of the seismic signal ~2 h long (Figure 4b), and then faded. A powerful, long-period (3–4 s) event was recorded at 13:05 (all times are UT) on 12 January 2006 at regional distances, and was located below the summit craters. It was associated with ash emission at the Bocca Nuova crater (Figure 1b), which occasionally had produced detonations linked to mild explosions since October 2005 [*Allard et al*., 2006]. Again, neither paroxysmal activity (e.g., lava fountains) nor lava emission was observed; however, in the wake of the long-period event, the RMS amplitude of the seismic signal dropped suddenly, returning to values comparable to those in the second half of November 2005 (Figure 3a).

4. Source Location of Volcanic Tremor

[6] Figures 5a and 5b shows the spectral characteristics of the signal at the vertical component of ECPN and ESPC from 00:00 on 16 December to midnight on 17 December, which is approximately 24 h before and after the abrupt enhancement in amplitude of volcanic tremor visible in Figure 4a. The spectrograms span from 0.24 to 15 Hz with a

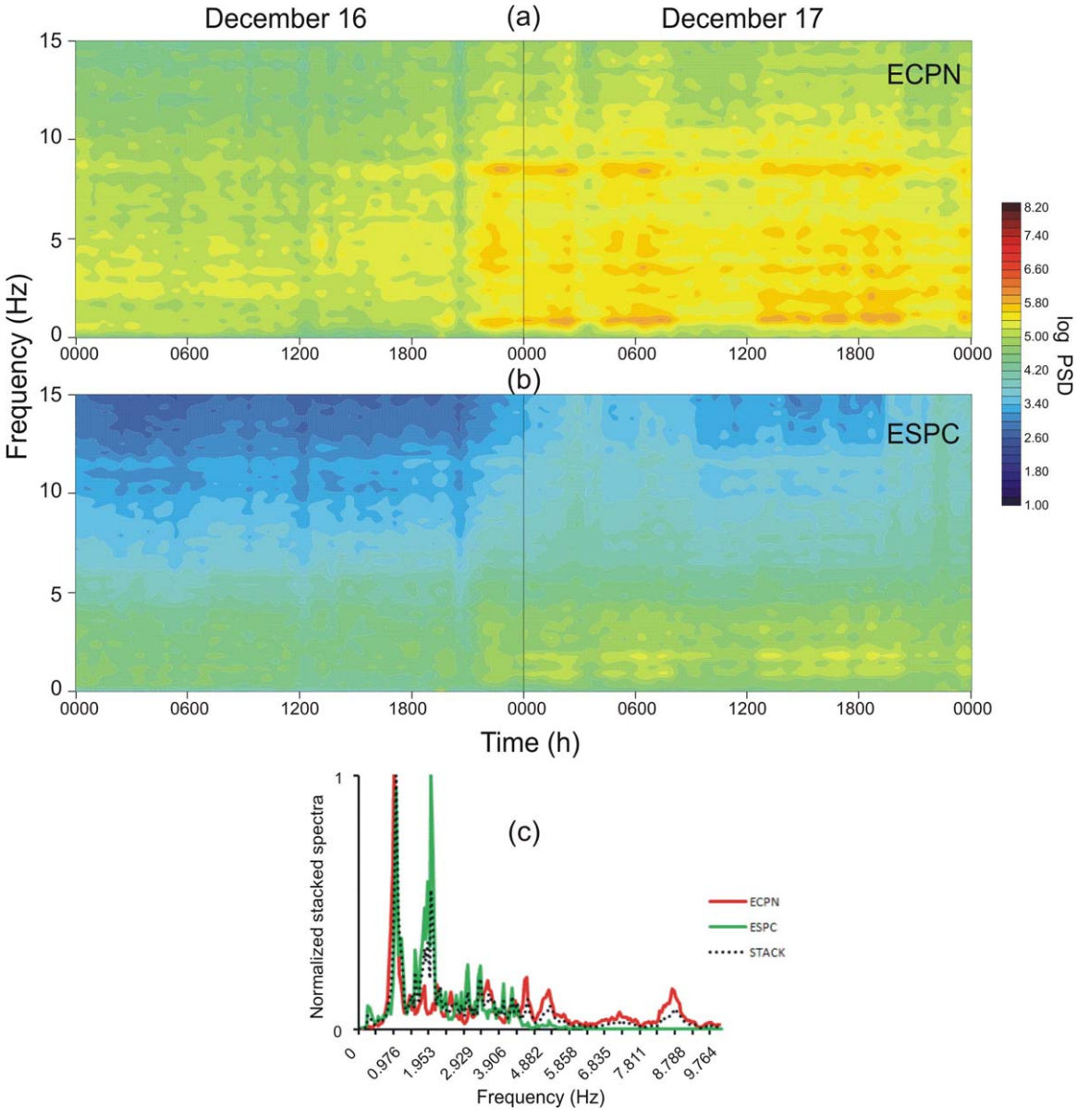

Figure 5. Power Spectral Density (PSD) of the seismic signal recorded at the vertical component of (a) ECPN and (b) ESPC from 16 to 17 December, 2005. The window length used for the spectra is 10.24 s with overlap of 50%. Amplitudes are in logarithmic scale. (c) Normalized stacked spectra at ECPN and ESPC in a 1 h long time span at the climax of the amplitude variation.

resolution of approximately 0.24 Hz, and were calculated over successive 1024 points (i.e., 10.24 s) with an overlap of 50%. Seismic radiation peaked at spectral frequencies between 0.8 and 8 Hz at ECPN, showing a broader spectrum than at distal stations like ESPC (0.7–4 Hz). The spectral energy peaked at 0.97 Hz, however, at both stations (Figure 5c) at the climax of the amplitude variation between 17 and 18 December, which is evidence of energy radiated from a common tremor source. Significant changes also occurred in the relative location and depth of the centroid of volcanic tremor. Following a 3-D grid search method proposed by *Di Grazia et al*. [2006], the centroid was calculated as a measure of the amplitude decay with distance, according to the general law $A(f, s) = A_o(f)\, s^{-b}\, e^{(-\alpha s)}$, where f is the frequency, s is the source-to-receiver distance, A_o is the amplitude of the signal generated at the source, b is a constant, and α is the frequency-dependent

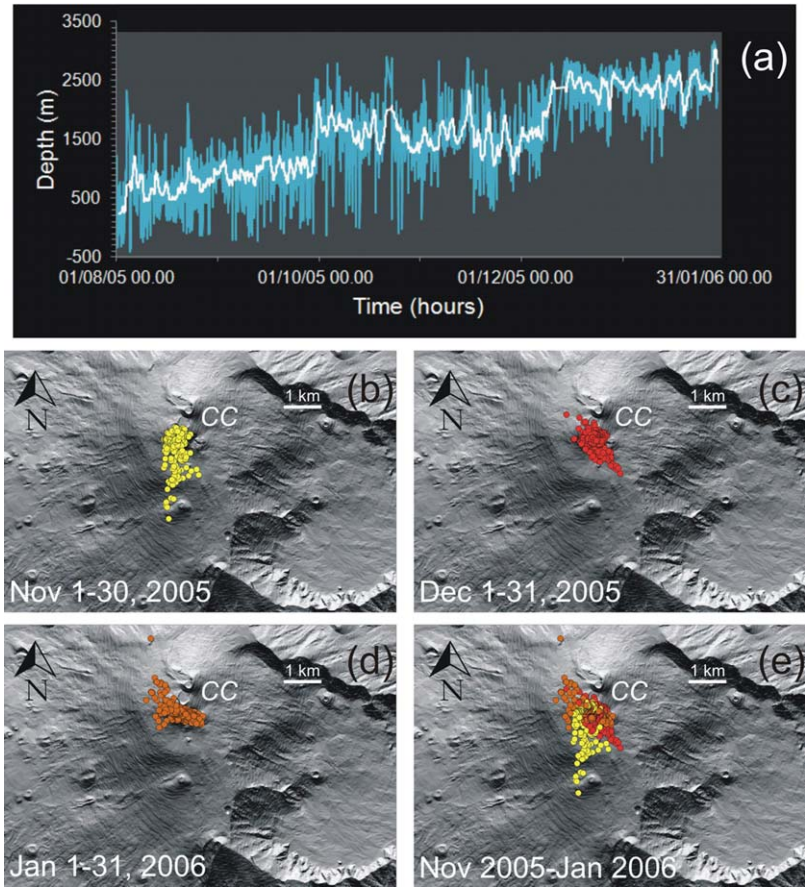

Figure 6. Centroid of volcanic tremor: (a) depths averaged over 1 h (light blue) and moving average over 24 h (white line) from August 2005 to January 2006. Location on a Digital Elevation Model of Mt. Etna in: (b) November 2005, (c) December 2005, (d) January 2006, and (e) altogether. CC stands for Central Craters. The dark grey rectangle in Figure 6a is depth below the summit of the volcano (~3330 m a.s.l).

absorption coefficient. We accepted a result only when: (i) at least 10 stations were available for the calculation, and (ii) the goodness of the regression fit (R^2) was $\geq$0.95. The calculation referred to a grid size of 6 $\times$ 6 km in horizontal and vertical direction, with a spacing of 250 m. The standard error for the set of computed locations was 370 m for latitude, 390 m for longitude, and 620 m for depth. This result is in the range of values (~400 m for latitude and longitude, and ~700 m for depth) obtained by *Di Grazia et al*. [2006] and *Patanè et al*. [2008], who assessed the stability of the centroid locations in 2004 and from October 2006 to December 2007, assuming similar values of R^2 and minimum number of stations for the computation.

[7] The migration of the centroid toward the surface began long before December (Figure 6a). The location moved from a minimum depth of ~400 m b.s.l. (on 5 August 2005) to ~3000 m a.s.l (on 31 January 2006, Figure 6e). Figure 7 offers an in-depth view of the relationships of depth versus longitude and latitude. About 95% of the centroid locations were up to 1500 m of elevation (within the volcano edifice) in August; the same percentage was between 1000 and 2500 m a.s.l. by the end of October. In addition, the locations became more clustered beneath the summit craters (Figure 7). Between 16 and 25 November, the centroid locations formed a branch elongated in the N-S direction, with extension of ~2.5 km from the summit craters (Figure 6b). The temporary shift was also evident from the major energy radiation recorded at EBEL with respect to ECPN (Figure 3a). Throughout December 2005 and January 2006, the centroids clustered in a predominantly NW-SE extension from the craters (Figures 6c–6d), and much closer to the surface (Figure 6a).

5. Pattern Classification

[8] Pattern classification can be described as the organization of data of any nature into groups

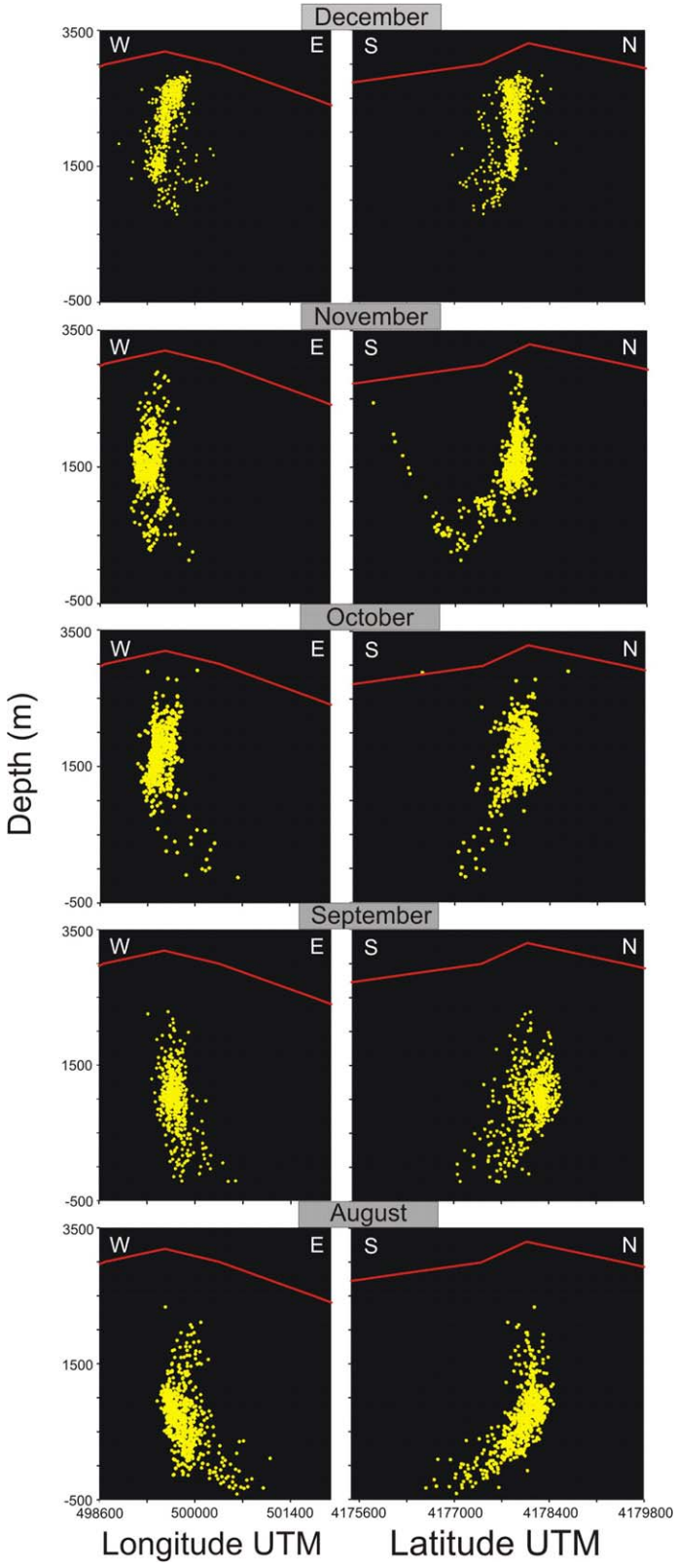

Figure 7. Depth versus (left) longitude and (right) latitude of the centroid of volcanic tremor from August to December 2005. The red silhouette in each cartoon marks the schematic topographic profile of the volcano.

sharing similar properties. Specific techniques, such as neural networks, Support Vector Machine, Hidden Markov Models, and hierarchical clustering, can be addressed to solve different classes of problems [e.g., *Duda et al*., 2001]. In volcano seismology, pattern classification has been successfully applied to data recorded at Soufriere Hills, Monserrat [*Rowe et al*., 2004; *Langer et al*., 2006], Stromboli [e.g., *Falsaperla et al*., 1996; *Esposito et al*., 2008], and Etna [e.g., *Masotti et al*., 2006; *Ibanez et al*., 2009; *Langer et al*., 2009]. Overall, the results obtained from the aforementioned applications highlighted good generalization capacities to distinguish transient events (e.g., earthquakes, explosion quakes, long-period events, and rock falls) as well as records of volcanic tremor associated with specific "states" of activity. Since 2010, automatic classification of volcanic tremor at Etna became a tool for 24/7 seismic surveillance in the control room of INGV-OE [*Langer et al*., 2011]. Named *KKAnalysis* [*Messina and Langer*, 2011], the software implemented at INGV-OE carries out the classification over 5 min of signal (see Appendix A), combining the results of Self-Organizing Maps (SOMs hereafter) and fuzzy clustering (software and documentation can be freely downloaded from http://earthref.org/ERDA/erda). The basic idea of this classification system in near real-time is that the level of volcano unrest is reflected in changes in amplitude and frequency content of the seismic signal, and a classifier trained to recognize different activity regimes (for example, quietness, strong Strombolian activity, paroxysms) can provide alarms when specific thresholds are reached [*D'Agostino et al*., 2012]. We applied *KKAnalysis* offline with the aim of: (i) exploring the characteristics of seismic signals never analyzed before with this tool, and (ii) comparing the results of pattern classification from November 2005 to January 2006 with those of patterns recorded during an eruptive phase occurred about 11 months later. In our study, *KKAnalysis* took into account spectral amplitude and frequency content of volcanic tremor over 5 min consecutive time spans. Accordingly, we preprocessed our seismic data calculating the power spectral density from 0.15 to 18 Hz. Each pattern was made up of spectral amplitudes measured in frequency bins of $\sim$ 0.29 Hz. Also note that the classifier carried out the partition of patterns into clusters by using fuzzy clustering. The number of clusters was defined a priori equal to three to be consistent with the results of *Langer et al*. [2011]. The results of SOM combined with fuzzy clustering at ECPN were depicted by using colored triangles to highlight the relationships among the patterns and their development in time (Figure 8). In this graphical format, similar colors inferentially indicate similar internal conditions of the system. The membership based on fuzzy clustering was scaled from 0 to 1, and depicted in Figure 8 as well. If a pattern belonged to one class only, then FC was 1 for that class and 0 for the remaining classes. Otherwise, the membership was expressed by a value between 0 and 1. In doing so, a measure of fuzziness (uncertainty) of the classification was provided for each pattern (see Appendix A).

[9] The beginning of November 2005 was characterized by cluster 1 and SOM green colors (Figure 8a). Repeated shifts between cluster 1 and 2 occurred in mid-November concurrent with the increase in the amplitude of volcanic tremor visible in Figure 3a. From 16 November onward, cluster 2 became quite stable over the following 30 days (Figure 8b). The change in amplitude of seismic radiation visible in the seismograms of Figure 4a was marked by a shift from cluster 2 to 3 during the night of 16 December, whilst the color of the triangles remained green (Figure 8c). With the beginning of the characteristic "banded tremor" (Figure 4b), the results of pattern classification showed a nearly regular swap between clusters 2 and 3, with an overall "comb" effect (Figure 8d). Yet, SOM colors remained green. By the beginning of January, cluster 3 completely disappeared, leaving a stable cluster 2 and SOM green colors until the end of the month. In order to allow the reader to compare the results obtained with those relative to eruptive stages, we also processed a 48 h time series recorded during the 2006 effusive activity and encompassing an episode of lava fountain. Figure 8e depicts the results of *KKAnalysis* starting about 26 h before the tremor buildup visible on seismogram at 02:09 on 24 November (see Figure 4c). Fuzzy clustering highlights a gradual change in the membership of patterns on 23 November (Figure 8e). SOM purple colors and cluster 2 characterize the pre-paroxysmal stage, whilst SOM pink colors and cluster 3 mark the paroxysm (Figure 8e).

6. VTs and Centroid Locations in Relation to Seismic Tomography

[10] High quality data recorded by the network of three-component seismometers permanently deployed on the volcano has fostered seismic

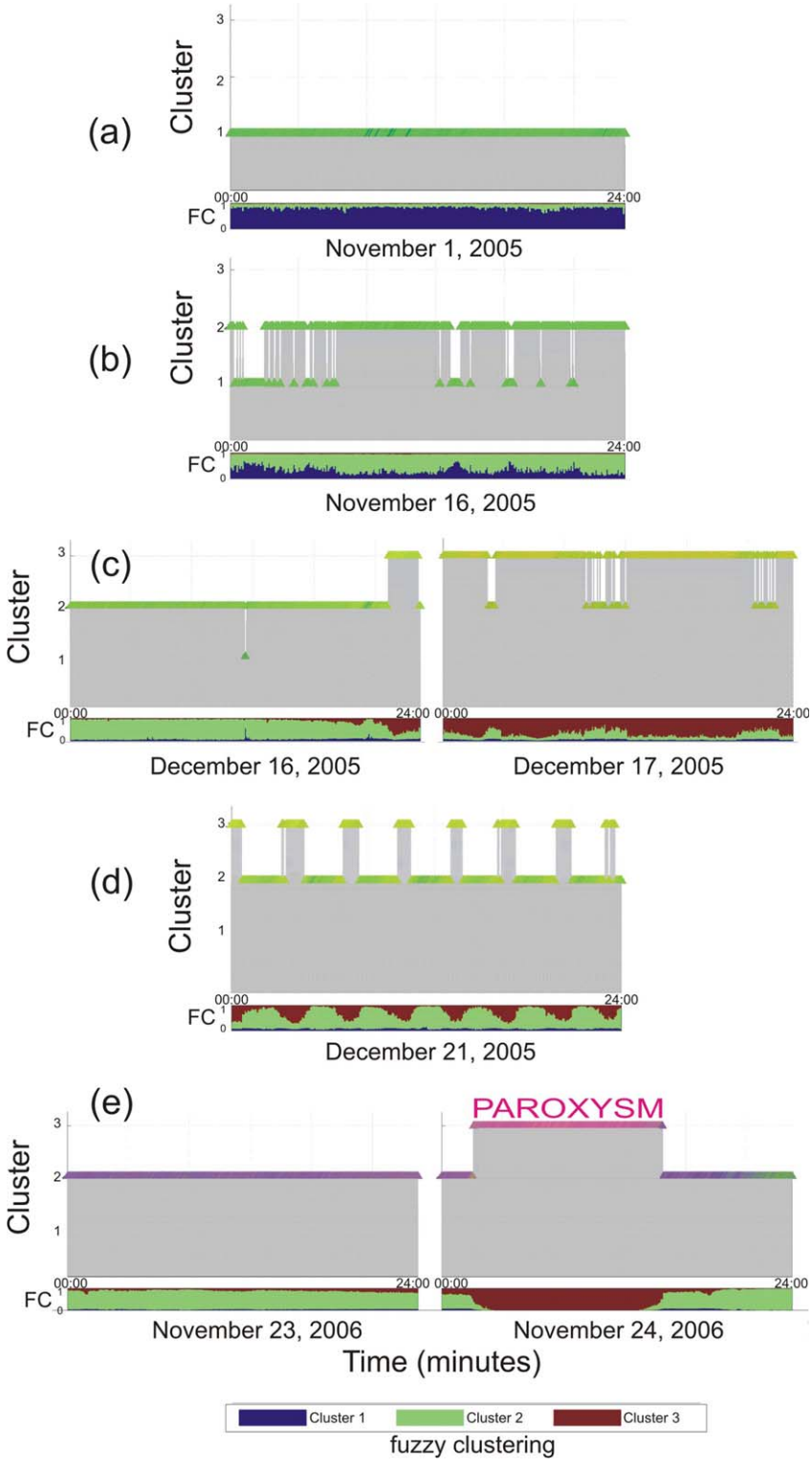

Figure 8. Pattern classification at ECPN from *KKAnalysis*. The results of SOM combined with fuzzy clustering are depicted as colored triangles. Time-ordered patterns in each panel cover 24 h. At the bottom of each panel from (a) to (e), the fuzzy clustering (FC) alone was also graphically depicted; the height of the color bar defines the degree of membership to a certain cluster. Figures 8a to 8d belong to our study period where no eruptive activity was observed. For comparison, in Figure 8e an example of pattern classification during an episode of effusive activity in November 2006 is depicted. In this case, purple triangles and cluster 2 prevail until the onset of the episode of lava fountain (paroxysm), which was marked by cluster 3 and SOM pink colors.

tomographic studies of the internal structure of Etna since the early 2000s [e.g., *Chiarabba et al*., 2000; *De Gori et al*., 2005], although investigations had begun as early as the 1990s [e.g., *Hirn et al*., 1991]. In the following, we refer our observations to the seismic tomography by *Patanè et al*. [2006], who defined a 3-D P-wave velocity structure of Mt. Etna, using VT earthquakes from 10 August 2001 to 18 January 2003, namely before and during the 2002–2003 flank eruption. A total of 712 earthquakes (8587 P- and 2293 S-wave arrivals) were inverted by *Patanè et al*. [2006] to model a grid $2 \times 2 \times 1$ km with SIMULPS-14 [*Thurber*, 1993], using the so called spread function (SF) as defined by *Michelini and McEvilly* [1991] to assess the quality of the results. In the 3-D model obtained by *Patanè et al*. [2006], a volume with relatively high P-wave velocity values was recognizable from sea level to 7 km b.s.l. This anomaly was also evident in previous tomographic studies, although variations in network configuration, data sets, and processing methods yielded a slightly different estimate of its spatial extent [*Chiarabba et al*., 2004, and references therein]. The high velocity body (HVB) was mostly aseismic, and was interpreted as solidified intrusive rock [*Chiarabba et al*., 2004, and references therein].

[11] Fracturing and fluids play an important role in affecting elastic parameters of rocks in volcanic environment. Changes in velocity anomalies may be indeed the results of material variations and modified environmental physical conditions. Consequently, we tried to verify whether or not the earthquake locations in our study support the existence of the aseismic anomalous region. In doing so, the hypocentral locations of 408 earthquakes recorded between July 2005 and January 2006 were calculated using SIMULPS-14 [*Thurber*, 1993] and the 3-D velocity model aforementioned. Then, we plotted the foci of the 408 earthquakes on the tomographic maps by *Patanè et al*. [2006]. One hundred and thirty-eight hypocenters with a depth greater than 7 km were excluded in order to focus on the regions with $SF \leq 2$, which—according to *Patanè et al*. [2006]—contoured well resolved zones obtained by the model (see white contours in Figure 9). We observed that there were no foci located inside the HVB, consistent with the aseismic characteristics of Patanè's HVB. Looking at the map from -2 to -6 km, we also noted that: (i) EBEL and ESPC were set above this volume and (ii) ECPN was at a greater distance from the top border of the HVB, despite its proximity to EBEL (Figure 9). Cross-sections provide more insight into the shape of this volume (Figure 10). In particular, oblique cross sections NW-SE and SW-NE oriented offer a completely new perspective of the HVB and its peculiar geometry (Figure 10a). The projection from each vertical section of the centroid locations of volcanic tremor is depicted within a distance of ± 0.7 km in Figure 10a, and of ± 1 km in Figure 10b. The black star is the center of each profile (value zero on each abscise) and corresponds to the center of the inversion grid (coordinates 37.733N–15E) located S of the central craters. In the oblique cross sections in Figure 10a, the majority of the centroid locations of volcanic tremor belong to A'A (3156 locations) and D'D (3654 locations), followed by B'B (572 locations) and E'E (64 locations). C'C contained only 1 centroid, whilst F'F had no centroid at all. For the W-E and S-N cross sections, 3643 locations in W-E (for $y = 2$) and 3709 locations in S-N (for $x = 0$) are found. The remaining part of centroid locations (less than 5% of the total number) belong to: W-E for $y = 0$ (85 locations), S-N for $x = -2$ (18 locations) and $x = 2$ (2 locations). Finally, there is no centroid in W-E for $y = -4$. Overall, the analysis of these sections highlights that: (i) the locations of the centroids of volcanic tremor were clustered above the upper northern border of the high velocity volume (see in particular A'A, S-N for $x = 0$, and W-E for $y = 2$), and (ii) ESPC was much closer to the top of this volume than the other two stations (see C'C, F'F in Figure 10a and W-E for $y = -4$, S-N for $x = 2$ in Figure 10b).

7. Discussion

[12] In order to analyze the variations in volcanic tremor during the second half of 2005, we tracked through time: the slow increase in the amplitude of the background seismic radiation up to a maximum of $\sim 1.9 \times 10^4$ nm/s at ECPN (Figures 2b and 3), the changes in the frequency content in mid-December (Figure 5), and the much shallower location of the centroid of volcanic tremor up to a few hundred meters below the surface (Figures 6 and 7). These changes came along with a large increase in SO_2 flux from fall 2005 onward (Figure 3b). The rise in SO_2 flux is recognized as one of the most diagnostic changes prior to magmatic eruptions [*Newhall*, 2007], even in cases of minimal VT seismicity and ground deformation in open conduit volcanoes, as observed at Mayon, Philippines [*Ramos-Villarta et al*., 1985] and

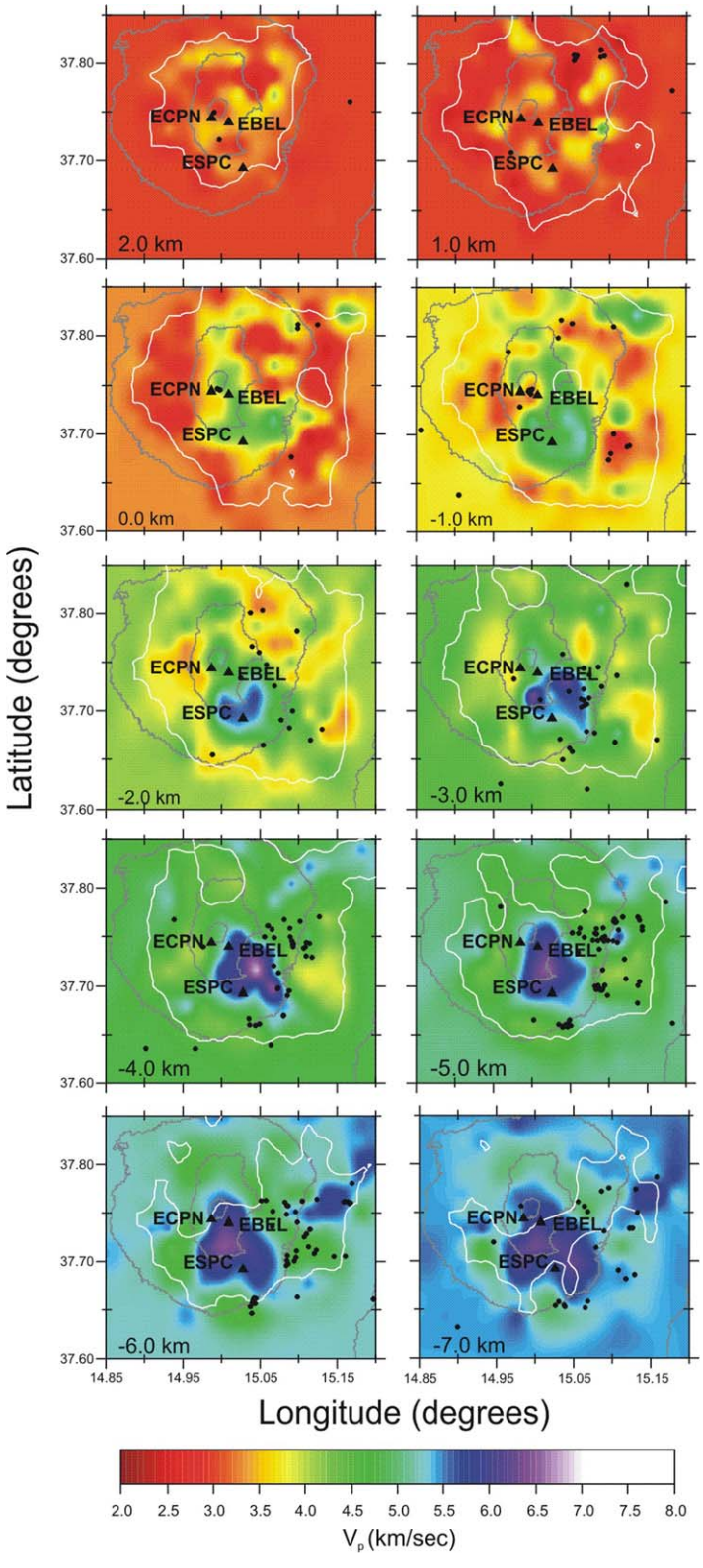

Figure 9. Location of earthquakes recorded from July 2005 to January 2006 superimposed on the seismic tomography of *Patanè et al*. [2006]. The maximum depth of the layers is up to 7 km b.s.l. to include the region bordered by white contours, for which the highest resolution of the model was obtained (SF ≤ 2). For each tomogram, the epicenters (solid black circles) are plotted relative to the depth indicated ± 0.5 km. Solid black triangles mark the location of the stations ECPN, EBEL, and ESPC.

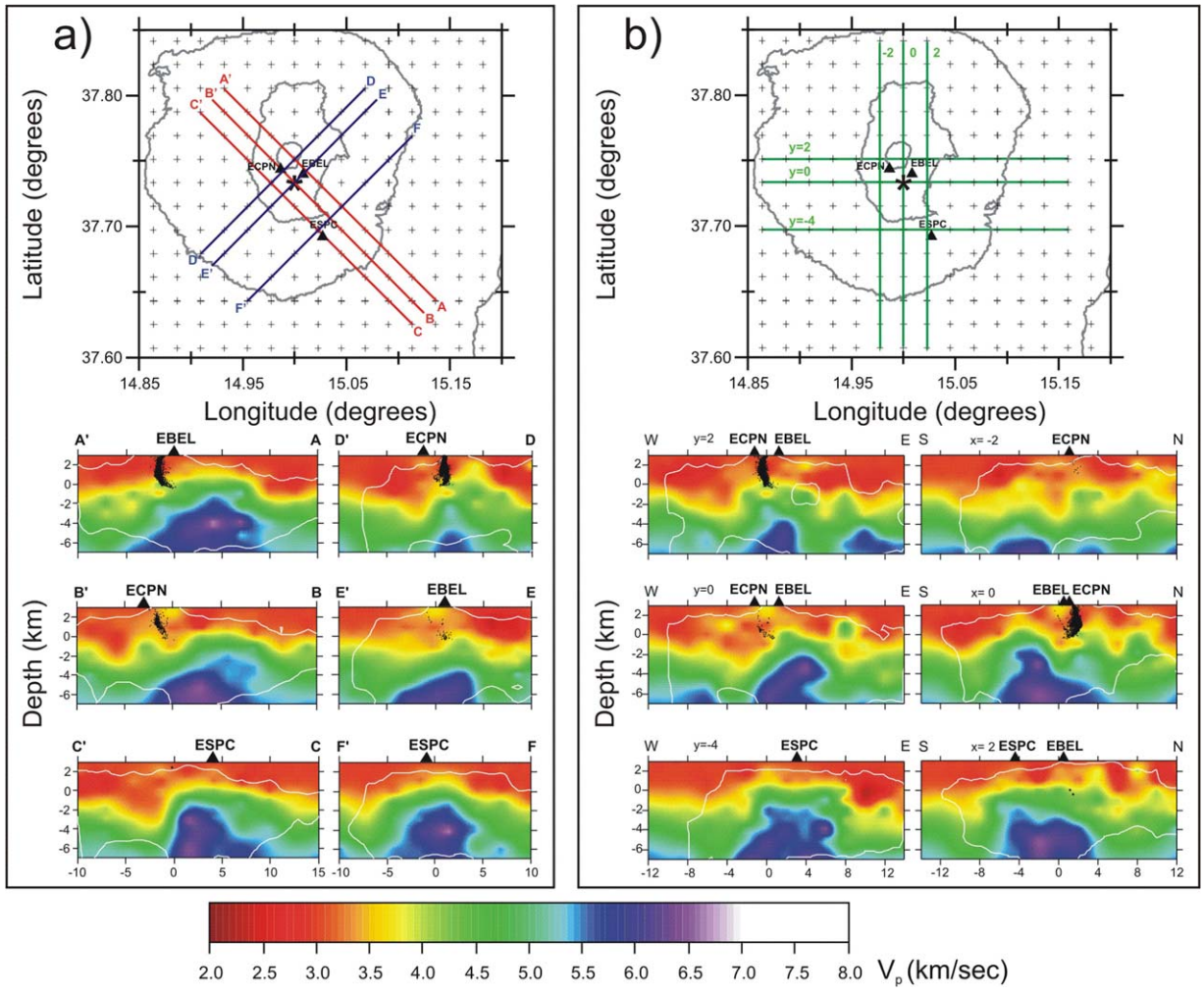

Figure 10. Cross sections of seismic tomography based on V_p: (a) NW-SE, SW-NE, and (b) W-E, S-N directions. The maps at the top of each panel indicate: the position of ECPN, EBEL, and ESPC (black triangles), the center of the inversion grid (black star), and the traces of the cross-sections (solid colored lines); crosses are the grid nodes used in the tomographic inversion. The white contours mark well-resolved regions with spread function SF ≤ 2. The projection of the centroids of volcanic tremor is depicted as black dots in each vertical section (see section 6 for details). Depth and horizontal distance in all cross sections are in kilometers.

Shishaldin [*Moran et al.*, 2006]. Etna has been instrumented with the FLAME (Flux Automatic Measurements) ultraviolet scanning DOAS network [*Salerno et al.*, 2009], which carries out measurements during daylight. Figure 3b shows the temporal evolution of the plume SO_2 flux from 1 June 2005 to 31 May 2006. The daily value increased at the beginning of November, reached a maximum ($\sim$10,000 Mg d^{-1}) in December, and then recovered its previous level in the late spring of 2006 (G. G. Salerno, personal communication, 2011). Despite the different sampling rate and scale of measure, there is an excellent correlation between the peak in the amplitude of volcanic tremor (Figure 3a) and in the SO_2 flux emission rate (Figure 3b). Overall, these observations suggested that a gradual recharging phase of the plumbing system started in mid-2005, approximately 5 months after the end of the 2004–2005 eruption (Figure 2b).

[13] Given these observations and the strong suggestion of magma influx at Etna, what was the reason for the eruption to fail? From pattern classification analysis (Figure 8), distinctive spectral characteristics with respect to those heralding eruptive conditions can be inferred. Even at the climax in December 2005, these characteristics

were far from those typical of volcanic tremor shortly before or during paroxysmal activity, as the comparison in Figures 8c–8e reveals. The results of the pattern classification, with the green color of patterns during the recharging (Figures 8c–8d), support the hypothesis that the magma remained at depth and did not enter in the shallow plumbing system (located from the surface up to ~3 km b.s.l., according to *De Gori et al*. [2005]). *Allard et al*. [2006] calculated that the magma which degassed between January 1993 and January 2005 had a volume of ~0.9 km^3, which corresponds to only 30% of the magma volumes eventually erupted. A previous evaluation for the years between 1975 and 1995 confirmed the voluminous portion of unerupted magma, with a value of the ratio of degassed to erupted magma equal to ~4 [*Allard*, 1997]. Our hypothesis that the shallow plumbing system remained unaffected by the magma recharging is also consistent with the mild inflation of the volcano summit documented by continuous GPS data (M. Mattia, personal communication, 2011) and with the negative mass changes calculated from gravimetric measurements. Density changes were computed by *Greco et al*. [2010] beneath an East-West profile along the southern flank of Etna from September 2004 to September 2006. Based on these gravity observations, *Greco et al*. [2010] obtained a rough estimate of the gain/loss of mass over time within the subsurface beneath the gravity stations. In the 2 year time span, their data highlighted a relative minimum in December 2005 (Figure 3c). An anticorrelated tremor/gravity anomaly was also found from 18 December 2005 and the first days of January 2006, using gravity measurements from a permanent spring gravimeter close to the summit craters [*Carbone et al*., 2008]. It is worth noting that banded tremor developed within this time span (Figures 4b and 8d). We surmise it was a consequence of periodic accumulations and discharges of gas, indicative of a relative equilibrium reached by gas supply within the volcanic system (see for example *Vergniolle and Jaupart* [1990]). VT seismicity likely disrupted this equilibrium when a seismic swarm in the depth range between 10 and 14 km b.s.l. affected the southern flank of the volcano on 8 January 2006 (supporting information Figure S1). *Cocina et al*. [2010] associated this swarm with a magmatic intrusion leading to the 2006 eruption. The swarm was followed by a powerful long-period event on 12 January and a sharp decrease in the volcanic tremor amplitude (Figure 3a). The volume of residual magma after the 2004–2005 was presumably small in the shallow plumbing system, according to the estimates by *Allard et al*. [2006]. Therefore, the new refilling at depth could not mobilize sufficient quantity of magma to erupt in the short term. Eruptive activity resumed only about 6 months later on 14 July, and continued until December 2006.

[14] The knowledge of the internal structure of Etna volcano has been progressively improved by geophysical investigations over the years. In the last decades, seismic tomography studies were carried out with various techniques, allowing the definition of a 3-D velocity structure of Etna to a depth of 18–24 km [*Chiarabba et al*., 2004, and reference therein]. The most important discovery was a high density cumulate and mainly aseismic body, extending S-SE from the summit craters and highly fractured in its western border, which according to *Chiarabba et al*. [2004] likely represented the preferential pathway for magma uprising during the 2001 lateral eruption. We surmise that the region of high density cracks likely played an important role in 2005 as well, driving to the surface the high flux of gas measured by the DOAS network. The oblique cross sections NW-SE and SW-NE oriented in Figure 10a document that the locations of the centroids of volcanic tremor in our study were clustered above the upper northern border of the HVB. In almost the same position, at a depth of ~3.5 km b.s.l., a vertically elongated pressurizing source was located by GPS data inversion from surveys carried out between 2005 and 2006 [*Bonforte et al*., 2008]. The oblique cross sections in Figure 10a also provide a clear image of the peculiar geometry of the HVB, which appears asymmetric and with its top much closer to ESPC than the other two stations. This is consistent with results obtained in previous studies, which documented that: (i) ESPC was "sensitive" to volcanic tremor changes [*Behncke et al*., 2009] and (ii) there were strong differences in the seismic energy radiation recorded at the two ECPN and EBEL stations, despite their almost comparable altitude and distance from the summit craters [*Falsaperla et al*., 2010].

8. Conclusions

[15] The conspicuous increase in volcanic tremor amplitude at the end of 2005 was linked to a recharging of the volcano feeder at depth. The results of the pattern classification unveiled that the seismic radiation had different spectral characteristics with respect to those observed during

eruptive periods. A pressure increase with no volume change was hypothesized, i.e., no magma intrusion within the shallow (<3 km b.s.l.) plumbing system in the investigated time span. Independent evidence of this comes from gravimetric measurements, which exclude a positive mass change, and from daily DOAS gas measurements, which documented an increase in the plume SO_2 flux concurrent with the peak in the amplitude of volcanic tremor. The refilling of gas was likely driven to the surface throughout a region of high density of cracks, which was the locus of intense seismicity (see Figure 9). This region surrounding the HVB imaged by seismic tomography [*Patanè et al*., 2006] has its apex beneath seismic station ESPC, while it is very distant from the summit station ECPN, located at a short distance from the active craters of Etna. The peculiar shape of the HVB would make ESPC "sensitive" to changes in the volcano feeder, and therefore an informative site in case of climactic activity.

[16] High-quality data acquired from the continuous monitoring of Mt. Etna, one of the most active volcanoes worldwide, forms a formidable base of knowledge on how volcanoes behave. The application of pattern classification methods, such as *KKAnalysis*, allows tracking subtle spectral changes in the seismic signal. The interpretation of internal dynamics in the light of multidisciplinary findings, such as those discussed in our study, is valuable: (i) to reduce the possibility of "false" eruption forecasts in the future and, in general, (ii) to improve our understanding of recharging and premonitory eruptive activity, useful in less monitored volcanic regions as well.

Appendix A: *KKAnalysis*, SOM, and Fuzzy Clustering

[17] *KKAnaysis* [*Messina and Langer*, 2011] exploits a collection of methods for unsupervised classification and clustering, using routines of the Self-Organizing Map (SOM) Toolbox 2 for MATLAB [*Vesanto et al*., 2000]. In particular, building upon the results obtained by *Langer et al*. [2011], we considered the combination of SOM and fuzzy clustering in our application to volcanic tremor data. A SOM is a type of artificial neural network proposed by *Kohonen* [2001] in which multidimensional data sets can be reduced in low dimensional spaces (e.g., 2-D diagrams), maintaining their topological relationships. The input data (called patterns) can be of any nature, and are presented to the classifier in numerical format as unlabeled data. Following *Langer et al*. [2009], the patterns of our study covered the spectral content up to 18 Hz of the seismic signal over 5 min, for a total of 288 patterns per day, which corresponded to 26,496 patterns from November 2005 to January 2006. Note that SOM have no expected-output target.

[18] SOMs are formed by nodes, representing a number of patterns. Our map consisted of $9 \times 47 = 423$ nodes using a lattice with hexagonal topology. Map geometry and size were fixed running principal component analysis within *KKAnalysis* (for an optimal design of SOMs, see *Vesanto et al*. [2000]). Node weights are adjusted iteratively at discrete time steps during the classification process. Accordingly, the sum of the distances between the original data and their representing prototype nodes converge to a minimum

$$D_{ij} = \sqrt{(\mathbf{W}_i - \mathbf{V}_j)^T (\mathbf{W}_i - \mathbf{V}_j)} \quad \text{(A1)}$$

where $\mathbf{V}_j$ is the normalized input feature vector and $\mathbf{W}_i$ the weights stored in the nodes. Throughout the classification process the upgrade of weights follows the relationship

$$\mathbf{W}_i(t+1) = \mathbf{W}_i(t) + \varphi(\Delta, t) \cdot \lambda(t) \cdot D_{ij}(t) \quad \text{(A2)}$$

where λ is the learning rate, and φ is the spatial influence parameter describing the dependence of upgrade on the distance Δ of a node from the best matching unit (BMU) for the j_{th} pattern. $\varphi\ (\Delta,t)$ has its maximum for the BMU, whereas nodes lying outside the radius of influence are not upgraded at all. The learning rate λ decreases during the training process and the parameter φ changes as the influence shrinks at any iteration step.

[19] In *KKAnalysis*, fuzzy clustering (FC) defines the allocation of patterns in each cluster. The class membership is given by a vector, the components of which can refer to different classes. In our study, a pattern was assigned to clusters 1, cluster 2, or cluster 3 on the basis of the largest component of the membership vector. The number of clusters was defined a priori equal to three to be consistent with the results of *Langer et al*. [2011]. The optimum partition is expressed by

$$J = \sum\nolimits_k J_k \quad \text{(A3)}$$

$$J_k = \sum\nolimits_i m_{ik}^q d_{ik}^2 \quad \text{(A4)}$$

where m_{ik} is the membership value of pattern i with respect to cluster k, d_{ik} is its Euclidean distance from the cluster centroid, and q (here $q = 2$) is a weighting exponent. The color bar for FC at the bottom of the diagrams in Figure 8 provides the complete representation of the fuzzy membership vectors for each pattern. Here blue, green,

and red correspond to clusters 1, 2, and 3, respectively, whereas the height of the colored field graphically depicts the degree of membership to a certain cluster.

[20] Running *KKAnalysis*, patterns were pooled together with a reference data set prepared by *Langer et al*. [2011], which pertained conditions from absent to paroxysmal volcanic activity in 2007–2008. Being processed together, the results of the classification of our data set could be compared with those related to eruptive episodes. This expedient was an elegant solution to use a priori knowledge in a context of learning by self-organization. The results from *KKAnalysis* were obtained in numerical format as well as color code in 2-D diagrams, mixing the principal colors RGB (red, green, and blue) according to node weights in the SOM. Colored triangles in Figure 8 were the combined results from SOM and fuzzy clustering, which were depicted as time-ordered patterns.

Acknowledgments

[21] We are grateful to: S. Alparone for sharing Figure 2b), M. Mattia for the fruitful discussions on GPS data, G. G. Salerno for the SO_2 data and F. Greco for the gravimetric data in Figure 3, A. Messina, H. Langer, and S. Spampinato for the software *KKAnalysis*, G. Di Grazia for the draft data of the centroid of the tremor source, S. Sicali and V. Milluzzo for sharing the pickings of VTs. We also acknowledge C. Rowe and A. Nercessian for their constructive comments.

References

Acocella, V., B. Behncke, M. Neri, and S. D'Amico (2003), Link between major flank slip and 2002–2003 eruption at Mt. Etna (Italy), *Geophys. Res. Lett.*, *30*(24), 2286, doi:10.1029/2003GL018642.

Allard, P. (1997), Endogenous magma degassing and storage at Mount Etna, *Geophys. Res. Lett.*, *24*, 2219–2222.

Allard, P., et al. (2006), Mount Etna 1993–2005: Anatomy of an evolving eruptive cycle, *Earth Sci. Rev.*, *78*, 85–114, doi:10.1016/j.earscirev.2006.04.002.

Aloisi, M., et al. (2009), A new dyke intrusion style for the Mount Etna May 2008 eruption modeled through continuous tilt and GPS data, *Terra Nova*, *21*, 316–321, doi:10.1111/j.1365-3121.2009.00889.x.

Andronico, D., et al. (2005), A multi-disciplinary study of the 2002–03 Etna eruption: Insights into a complex plumbing system, *Bull. Volcanol.*, *67*, 314–330, doi:10.1007/s00445-004-0372-8.

Behncke, B., and M. Neri (2003a), The July–August 2001 eruption of Mt. Etna (Sicily), *Bull. Volcanol.*, *65*, 461–476, doi:10.1007/s00445-003-0274-1.

Behncke, B., and M. Neri (2003b), Cycles and trends in the recent eruptive behaviour of Mount Etna (Italy), *Can. J. Earth Sci.*, *40*, 1405–1411, doi:10.1139/E03-052.

Behncke, B., S. Falsaperla, and E. Pecora (2009), Complex magma dynamics at Mount Etna revealed by seismic, thermal and volcanological data, *J. Geophys. Res.*, *114*, B03211, doi:10.1029/2008JB005882.

Bonforte, A., et al. (2008), Feeding system and magma storage beneath Mt. Etna as revealed by recent inflation/deflation cycles, *J. Geophys. Res.*, *113*, B05406, doi:10.1029/2007JB005334.

Burton, M., et al. (2005), Etna 2004–2005: An archetype for geodynamically controlled effusive eruptions, *Geophys. Res. Lett.*, *32*, L09303, doi:10.1029/2005GL022527.

Cannata, A., et al. (2009), Long period and very long period events at Mt. Etna volcano: Characteristics, variability and causality, and implications for their sources, *J. Volcanol. Geotherm. Res.*, *187*, 227–249.

Carbone, D., L. Zuccarello, and G. Saccorotti (2008), Geophysical indications of magma uprising at Mt Etna during the December 2005 to January 2006 non-eruptive period, *Geophys. Res. Lett.*, *35*, L06305, doi:10.1029/2008GL033212.

Chiarabba, C., A. Amato, E. Boschi, and F. Barberi (2000), Recent seismicity and tomographic modeling at Mount Etna plumbing system, *J. Geophys. Res.*, *105*, 10,923–10,938, doi:10.1029/1999JB900427.

Chiarabba, C., P. De Gori, and D. Patanè (2004), The Mt. Etna plumbing system: The contribution of seismic tomography, in *Mt Etna Volcano Laboratory, Geophysics Monograph Series*, vol. *143*, edited by A. Bonaccorso et al., pp. 191–204, AGU, Washington, D. C.

Cocina, O., et al. (2010), Seismic activity at Mt. Etna from July 2005 to January 2006: Evidence of a deep magmatic intrusion leading to the 2006 eruption, *Geophys. Res. Abstr.*, vol. *12*, EGU2010–9267, EGU General Assembly, Vienna, 2–7 May 2010.

D'Agostino, M., et al. (2012), Volcano monitoring and early warning on Mt Etna based on volcanic tremor—Methods and technical aspects, in *Complex Monitoring of Volcanic Activity: Methods and Results*, edited by V. Zobin, Nova Science, Hauppage, NY, USA.

De Gori, P., C. Chiarabba, and D. Patané (2005), Qp structure of Mount Etna: Constraints for the physics of the plumbing system, *J. Geophys. Res.*, *110*, B05303, doi:10.1029/2003JB002875.

Di Grazia, G., S. Falsaperla, and H. Langer (2006), Volcanic tremor location during the 2004 Mount Etna lava effusion, *Geophys. Res. Lett.*, *33*, L04304, doi:10.1029/2005GL025177.

Di Grazia, G., et al. (2009), A multiparameter approach to volcano monitoring based on 4D analyses of seismo-volcanic and acoustic signals: The 2008 Mt. Etna eruption, *Geophys. Res. Lett.*, *36*, L18307, doi:10.1029/2009GL039567.

Doglioni, C., F. Innocenti, and G. Mariotti (2001), Why Mt Etna?, *Terra Nova*, *13*, 25–31.

Duda, R. O., P. E. Hart, and D. G. Stork (2001), *Pattern Classification*, 2nd ed., John Wiley, NY, USA.

Esposito, A. M., et al. (2008), Unsupervised neural analysis of very-long-period events at Stromboli volcano using the Self-Organizing Maps, *Bull. Seismol. Soc. Am.*, *98*(5), 2449–2459, doi:10.1785/0120070110.

Falsaperla, S., S. Graziani, G. Nunnari, and S. Spampinato (1996), Automatic classification of volcanic earthquakes by using multi-layered neural networks, *Nat. Hazards*, *13*, 205–228.

Falsaperla, S., et al. (2010), Effects of the 1989 fracture system in the dynamics of the upper SE flank of Etna revealed by volcanic tremor data: The missing link?, *J. Geophys. Res.*, *115*, B11306, doi:10.1029/2010JB007529.

Greco, F., et al. (2010), Spatiotemporal gravity variations to look deep into the southern flank of Etna volcano, *J. Geophys. Res.*, *115*, B11411, doi:10.1029/2009JB006835.

Gvirtzman, Z., and A. Nur (1999), The formation of Mount Etna as the consequence of slab rollback, *Nature*, *401*, 782–785.

Hirn, A., et al. (1991), Seismic heterogeneity of Mt. Etna: Structure and activity, *Geophys. J. Int.*, *105*, 139–153, doi: 10.1111/j.1365-246X.1991.tb03450.x.

Hirn, A., R. Nicolich, J. Gallart, M. Laigle, and ETNASEIS Scientific Group (1997), Roots of Etna volcano in faults of great earthquakes, *Earth Planet. Sci. Lett.*, *148*, 171–191.

Ibanez, J. M., et al. (2009), The classification of seismo-volcanic signals using Hidden Markov Models as applied to the Stromboli and Etna volcanoes, *J. Volcanol. Geotherm. Res.*, *187*, 218–226.

Kieffer, S. (1984), Seismicity at old faithful geyser: An isolated source of geothermal noise and possible analogue of volcanic seismicity, *J. Volcanol. Geotherm. Res.*, *22*, 59–95.

Kohonen, T. (2001), *Self Organizing Maps*, 3rd ed., 501 pp., Springer, Berlin.

Langer, H., S. Falsaperla, T. Powell, and G. Thompson (2006), Automatic classification and a-posteriori analysis of seismic event identification at Soufriere Hills volcano, Montserrat, *J. Volcanol. Geotherm. Res.*, *153*, 1–10, doi:10.1016/j.jvolgeores.2005.08.012.

Langer, H., et al. (2009), Synopsis of supervised and unsupervised pattern classification techniques applied to volcanic tremor data at Mt. Etna, Italy, *Geophys. J. Int.*, *178*, 1132–1144, doi:10.1111/j.1365-246X.2009.04179.x.

Langer, H., et al. (2011), Detecting imminent eruptive activity at Mt Etna, Italy, in 2007–2008 through pattern classification of volcanic tremor data, *J. Volcanol. Geotherm. Res.*, *200*, 1–17, doi:10.1016/j.jvolgeores.2010.11.019.

Masotti, M., et al. (2006), Application of support vector machine to the classification of volcanic tremor at Etna, Italy, *Geophys. Res. Lett.*, *33*, L20304, doi:10.1029/2006GL027441.

McNutt, S. R. (1992), Volcanic tremor, in *Encyclopedia of Earth System Science*, vol. *4*, pp. 417–425, Academic Press, San Diego, Calif.

McNutt, S. R. (2000), Volcanic seismicity, in *Encyclopedia of Volcanoes*, edited by H. Sigurdsson, et al., pp. 1095–1119, Academic, San Diego, Calif.

Messina, A., and H. Langer (2011), Pattern recognition of volcanic tremor data on Mt Etna (Italy) with KKAnalysis—A software for unsupervised classification, *Comput. Geosci.*, *37*, 953–961, doi:10.1016/j.cageo.2011.03.015.

Michelini, A., and T. V. McEvilly (1991), Seismological studies at Parkfield. I. Simultaneous inversion for velocity structure and hypocenters using cubic b-spline parameterization, *Bull. Seismol. Soc. Am.*, *81*, 524–552.

Moran, S. C., O. Kwoun, T. Masterlark, and Z. Lu (2006), On the absence of INSAR-detected volcano deformation spanning the 1995–1996 and 1999 eruptions of Shishaldin Volcano, Alaska, *J. Volcanol. Geotherm. Res.*, *150*, 119–131.

Moran, S. C., C. Newhall, and D. C. Roman (2011), Failed magmatic eruptions: Late-stage cessation of magma ascent, in Failed Eruptions: Late-Stage Cessation of Magma Ascent, edited by S. C. Moran, C. G. Newhall, D. C. Roman, *Bull. Volcanol.*, *73*(2), 115–122.

Neri, M., et al. (2009), Deformation and eruptions at Mt. Etna (Italy): A lesson from 15 years of observations, *Geophys. Res. Lett.*, *36*, L02309, doi:10.1029/2008GL036151.

Newhall, C. G. (2007), Volcanology for seismologists, in *Treatise on Geophysics*, vol. *4*, edited by G. Schubert and H. Kanamori, pp. 351–388, Elsevier.

Patanè, D., et al. (2006), Time resolved seismic tomography detects magma intrusions at Mount Etna, *Science*, *313*, 821–823.

Patanè, D., et al. (2008), Shallow magma pathway geometry at Mt. Etna volcano, *Geochem. Geophys. Geosyst.*, *9*, Q12021, doi:10.1029/2008GC002131.

Poland, M. (2010), Learning to recognize volcanic non-eruptions, *Geology*, *38*, 287–288, doi:10.1130/focus032010.1.

Ramos-Villarta, S., E. Corpuz, and C. G. Newhall (1985), Eruptive history of Mayon Volcano, Philippines, *Philipp. J. Volcanol.*, *2*, 1–35.

Rowe, C. A., C. H. Thurber, and R. A. White (2004), Dome growth behavior at Soufriere Hills Volcano, Montserrat, revealed by relocation of volcanic event swarms, 1995–1996, *J. Volcanol. Geotherm. Res.*, *134*, 199–221.

Salerno, G. G., et al. (2009), Three-years of SO_2 flux measurements of Mt. Etna using an automated UV scanner array: Comparison with conventional traverses and uncertainties in flux retrieval, *J. Volcanol. Geotherm. Res.*, *183*, 76–83.

Solaro, G., et al. (2010), Anatomy of an unstable volcano from InSAR: Multiple processes affecting flank instability at Mt. Etna, 1994–2008, *J. Geophys. Res.*, *115*, B10405, doi: 10.1029/2009JB000820.

Thurber, C. H. (1993), Local earthquake tomography: Velocities and Vp/Vs theory, in *Seismic Tomography: Theory and Practise*, edited by H. M. Iyer, K. Hirahara, pp. 563–583, Chapman and Hall, New York.

Vergniolle, S., and C. Jaupart (1990), Dynamics of degassing at Kilauea Volcano, Hawaii, *J. Geophys. Res.*, *95*, 2793–2809.

Vesanto, J., J. Himberg, E. Alhoniemi, and J. Parhankangas (2000), SOM Toolbox for Matalab 5, Rep. A57. [Available at http://www.cis.hut.fi/projects/somtoolbox.].

Walter, T. R., V. Acocella, M. Neri, and F. Amelung (2005), Feedback processes between magmatic events and flank movement at Mount Etna (Italy) during the 2002–2003 eruption, *J. Geophys. Res.*, *110*, B10205, doi:10.1029/2005JB003688.

Zadeh, L. A. (1965), Fuzzy sets, *Inf. Control*, *8*, 338–353.